Journal of Science and Technology in Civil Engineering NUCE 2019. 13 (3): 124–134

# SCALED BOUNDARY FINITE ELEMENT METHOD WITH CIRCULAR DEFINING CURVE FOR GEO-MECHANICS APPLICATIONS

Nguyen Van Chung[a]

[a]*Faculty of Civil Engineering, HCMC University of Technology and Education, No 1 Vo Van Ngan street, Thu Duc district, Ho Chi Minh city, Vietnam*

***Article history:***
*Received 06/08/2019, Revised 27/08/2019, Accepted 28/08/2019*

**Abstract**

This paper presents an efficient and accurate numerical technique based upon the scaled boundary finite element method for the analysis of two-dimensional, linear, second-order, boundary value problems with the domain completely described by a circular defining curve. The scaled boundary finite element formulation is established in a general framework allowing single-field and multi-field problems, bounded and unbounded bodies, distributed body source, and general boundary conditions to be treated in a unified fashion. The conventional polar coordinates together with a properly selected scaling center are utilized to achieve the exact description of the circular defining curve, exact geometry of the domain, and exact spatial differential operators. A general solution of the resulting system of linear, second-order, nonhomogeneous, ordinary differential equations is constructed via standard procedures and then used together with the boundary conditions to form a system of linear algebraic equations governing nodal degrees of freedom. The computational performance of the implemented procedure is then fully investigated for various scenarios within the context of geo-mechanics applications.

*Keywords:* exact geometry; geo-mechanics; multi-field problems; SBFEM; scaled boundary coordinates.

https://doi.org/10.31814/stce.nuce2019-13(3)-12 

## 1. Introduction

In the past two decades, the scaled boundary finite element method (SBFEM) has been developed for unbounded and bounded domains in two and three-dimensional media. The SBFEM is achieved in two purposes such with regards to the analytical and numerical method and to the standard procedure of the finite element and boundary element method within the numerical procedures [1]. The SBFEM has proved to be more general than initially investigated, then developments have allowed analysis of incompressible material and bounded domain [2], and inclusion of body loads [3]. The complexity of the original derivation of this technique led to develop weighted residual formulation [4, 5]. Then [6, 7] used virtual work and novel semi-analytical approach of the scaled boundary finite element method to derive the standard finite element method for two dimensional problems in solid mechanics accessibly.

Vu and Deeks [8] investigated high-order elements in the SBFEM. The spectral element and hierarchical approach were developed in this study. They found that the spectral element approach was

*Corresponding author. *E-mail address:* chungnv@hcmute.edu.vn (Chung, N. V.)

better than the hierarchical approach. Doherty and Deeks [9] developed a meshless scaled boundary method to model the far field and the conventional meshless local Petrov-Galerkin modeling. This combining was general and could be employed to other techniques of modeling the far field. Although, the SBFEM has demonstrated many advantages in the approach method, it also has had disadvantaged in solving problems involving an unbounded domain or stress singularities. When the number of degrees of freedom became too large, the computational expense was a trouble. So, He et al. [10] developed a new Element-free Galerkin scaled boundary method to approximate in the circumferential direction. This work was applied to a number of standard linear elasticity problems, and the technique was found to offer higher and better convergence than the original SBFEM. Furthermore, Vu and Deeks [11] presented a p-adaptive in the SBFEM for the two dimensional problem. These authors investigated an alternative set of refinement criteria. This led to be maximized the solution accuracy and minimizing the cost. Additionally, He et al. [12] investigated the possibility of using the Fourier shape functions in the SBFEM to approximate in the circumferential direction. This research used to solve three elastostactic and steady-state heat transfer problems. They found that the accuracy and convergence were better than using polynomial elements or using an element-free Galerkin to approximate on the circumferential direction in the SBFEM. In nearly years, [13] presented an exact defining curves for two-dimensional linear multi-field media. These authors selected the scaling center are utilized to achieve the exact description of circular defining curve, exact geometry of domain, and exact spatial differential operators. They showed that use the exact description of defining curve in the solution procedure can significantly reduce the solution error and, as a result, reduce the number of degrees of freedom required to achieve the target accuracy in comparison with standard linear elements.

The aforementioned works have shown various important progresses to implement the SBFEM in analysis of engineering problems. In geotechnical engineering, bearing capacity and slope stability problems are of very particular importance. When a mass of soil is loaded, it displays behavioral complexities, which may depend on stress or strain levels. The objective of this study is to extend the work of Jaroon and Chung [13] to further enhance the capability of the SBFEM with circular defining curve to analyze geo-mechanics in unbounded bodies. The medium is made of a homogeneous, linearly elastic material. The conventional polar coordinates are used to discretize on the defining curve. The paper is organized as follows. Section 2 deals with the weak-form equation of two-dimensional, multi-filed body. Section 3 addresses the SBFEM formulation and solution. Finally, the presented formulation will be used for analysis of two examples in Section 4 followed by conclusions drawn from this study in Section 5.

## 2. Problem formulation

Consider a two-dimensional body occupying a region $\Omega$ in $R^2$ as shown schematically in Fig. 1. The region is assumed smooth in the sense that all involved mathematical operators (e.g., integrations and differentiations) can be performed over this region. In addition, the boundary of the body $\Omega$, denoted by $\partial\Omega$, is assumed piecewise smooth and an outward unit normal vector at any smooth point on $\partial\Omega$ is denoted by $\mathbf{n} = \{n_1 \;\; n_2\}^T$. The interior of the body is denoted by $\text{int}\,\Omega$.

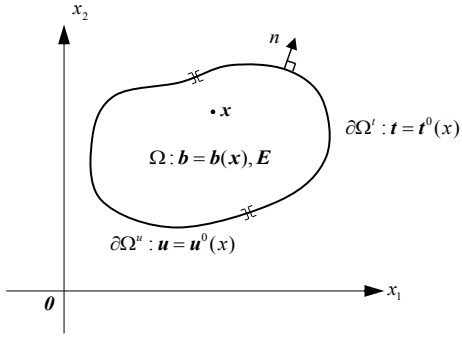


Figure 1. Schematic of two-dimensional, multi-field body

Three basic field equations including the fundamental law of conservation, the constitutive law of materials, and the relation between the state variable and its measure of variation, which relate the three field quantities $\mathbf{u}(\mathbf{x})$, $\bar{\boldsymbol{\varepsilon}}(\mathbf{x})$ and $\boldsymbol{\sigma}(\mathbf{x})$, are given explicitly by

$$\mathbf{L}^T\boldsymbol{\sigma} + \mathbf{b} = \mathbf{0} \tag{1}$$

$$\boldsymbol{\sigma} = \boldsymbol{D}\bar{\boldsymbol{\varepsilon}} \tag{2}$$

$$\bar{\boldsymbol{\varepsilon}} = \mathbf{L}\mathbf{u} \tag{3}$$

where $\mathbf{L}$ is a linear differential operator defined, in terms of a $2\Lambda \times \Lambda$-matrix, by

$$\mathbf{L} = \mathbf{L}_1\frac{\partial}{\partial x_1} + \mathbf{L}_2\frac{\partial}{\partial x_2};\ \mathbf{L}_1 = \begin{bmatrix}\mathbf{I}\\ \mathbf{0}\end{bmatrix}, \mathbf{L}_2 = \begin{bmatrix}\mathbf{0}\\ \mathbf{I}\end{bmatrix} \tag{4}$$

with $\mathbf{I}$ and $\mathbf{0}$ denoting a $\Lambda \times \Lambda$-identity matrix and a $\Lambda \times \Lambda$-zero matrix, respectively. By applying the law of conservation at any smooth point $\mathbf{x}$ on the boundary $\partial\Omega$, the surface flux $\mathbf{t}(\mathbf{x})$ can be related to the body flux $\boldsymbol{\sigma}(\mathbf{x})$ and the outward unit normal vector $\mathbf{n}(\mathbf{x})$ by $\mathbf{t} = \begin{bmatrix} n_1\mathbf{I} & n_2\mathbf{I}\end{bmatrix}\boldsymbol{\sigma}$, where, $n_1$ and $n_2$ are components of $\mathbf{n}(\mathbf{x})$.

By applying the standard weighted residual technique to the law of conservation in Eq. (1), then integrating certain integral by parts via Gauss-divergence theorem, and finally employing the relations in Eqs. (2) and (3), the weak-form equation in terms of the state variable is given by

$$\int_\Omega (\mathbf{L}\mathbf{w})^T\mathbf{D}(\mathbf{L}\mathbf{u})dA = \int_{\partial\Omega}\mathbf{w}^T\mathbf{t}dl + \int_\Omega \mathbf{w}^T\mathbf{b}dA \tag{5}$$

where $\mathbf{w}$ is a $\Lambda$-component vector of test functions satisfying the integrability condition $\int_\Omega \left[(\mathbf{L}\mathbf{w})^T(\mathbf{L}\mathbf{w}) + \mathbf{w}^T\mathbf{w}\right]dA < \infty$.

## 3. Scaled boundary formulation

Let $\mathbf{x}_0 = (x_{10}, x_{20})$ be a point in $R^2$ and $C$ be a simple, piecewise smooth curve in $R^2$ parameterized by a function $\mathbf{r} : s \in [a, b] \rightarrow (x_{10} + \hat{x}_1(s), x_{20} + \hat{x}_2(s)) \in R^2$ as shown in Fig. 2. Now, let us introduce the following coordinate transformation

$$x_\alpha = x_{\alpha 0} + \xi\hat{x}_\alpha(s) \tag{6}$$

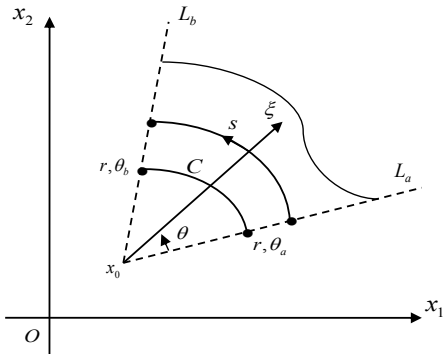


Figure 2. Schematic of a scaling center $\mathbf{x}_0$ and a defining curve $C$

where

$$\hat{x}_1(s) = r\cos\left(\theta_a\frac{(1-s)}{2} + \theta_b\frac{(1+s)}{2}\right);\ \hat{x}_2(s) = r\sin\left(\theta_a\frac{(1-s)}{2} + \theta_b\frac{(1+s)}{2}\right) \tag{7}$$

The linear differential operator $\mathbf{L}$ given by Eq. (4) can now be expressed in terms of partial derivatives with respect to $\xi$ and $s$ by

$$\mathbf{L} = \mathbf{b}_1\frac{\partial}{\partial\xi} + \mathbf{b}_2\frac{1}{\xi}\frac{\partial}{\partial s} \tag{8}$$

where $\mathbf{b}_1$ and $\mathbf{b}_2$ are $2\Lambda \times \Lambda$-matrices defined by

$$\mathbf{b}_1 = \frac{1}{J}\begin{bmatrix} \dfrac{d\hat{x}_2}{ds}\mathbf{I}_{\Lambda\times\Lambda} \\ -\dfrac{d\hat{x}_1}{ds}\mathbf{I}_{\Lambda\times\Lambda} \end{bmatrix}; \quad \mathbf{b}_2 = \frac{1}{J}\begin{bmatrix} -\hat{x}_2\mathbf{I}_{\Lambda\times\Lambda} \\ \hat{x}_1\mathbf{I}_{\Lambda\times\Lambda} \end{bmatrix}; \quad J = \hat{x}_1\frac{d\hat{x}_2}{ds} - \hat{x}_2\frac{d\hat{x}_1}{ds} \tag{9}$$

(for more details about the description of circular arc element, see also the work of [13]).

From the coordinate transformation along with the approximation, the state variable $\mathbf{u}$ is now approximated by $\mathbf{u}^h$ in a form

$$\mathbf{u}^h = \mathbf{u}^h(\xi, s) = \sum_{i=1}^{m} \boldsymbol{\phi}_{(i)}(s)\mathbf{u}^h_{(i)}(\xi) = \mathbf{N}^S\mathbf{U}^h \tag{10}$$

where $\mathbf{u}^h_{(i)}(\xi)$ denotes the value of the state variable along the line $s = s_{(i)}$, $\mathbf{N}^S$ is a $\Lambda \times m\Lambda$-matrix containing all basis functions, and $\mathbf{U}^h$ is a vector containing all functions $\mathbf{u}^h_{(i)}(\xi)$. The approximation of the body flux $\boldsymbol{\sigma}$ is given by

$$\boldsymbol{\sigma}^h = \boldsymbol{\sigma}^h(\xi, s) = \mathbf{D}(\mathbf{L}^h\mathbf{u}^h) = \mathbf{D}\left[\mathbf{B}_1\mathbf{U}^h_{,\xi} + \frac{1}{\xi}\mathbf{B}_2\mathbf{U}^h\right] \tag{11}$$

where $\mathbf{B}_1$ and $\mathbf{B}_2$ are given by $\mathbf{B}_1 = \mathbf{b}_1\mathbf{N}^S$; $\mathbf{B}_2 = \mathbf{b}_2\mathbf{B}^S$; $\mathbf{B}^S = d\mathbf{N}^S/ds$. Similarly, the weight function $\mathbf{w}$ and its derivatives $\mathbf{Lw}$ can be approximated, in a similar fashion, by

$$\mathbf{w}^h = \mathbf{w}^h(\xi, s) = \sum_{i=1}^{m} \boldsymbol{\phi}_{(i)}(s)\mathbf{w}^h_{(i)}(\xi) = \mathbf{N}^S\mathbf{W}^h \tag{12}$$

where $\mathbf{w}^h_{(i)}(\xi)$ denotes an arbitrary function of the coordinate $\xi$ along the line $s = s_{(i)}$ and $\mathbf{W}^h$ is a vector containing all functions $\mathbf{w}^h_{(i)}(\xi)$.

A set of scaled boundary finite element equations is established for a generic, two-dimensional body $\Omega$ as shown in Fig. 3. The boundary of the domain $\partial\Omega$ is assumed consisting of four parts resulting from the scale boundary coordinate transformation with the scaling center $\mathbf{x}_0$ and defining curve $C$: the inner boundary $\partial\Omega_1$, the outer boundary $\partial\Omega_2$, the side-face-1 $\partial\Omega^s_1$, and the side-face-2 $\partial\Omega^s_2$. The body is considered in this general setting to ensure that the resulting formulation is applicable to various cases.

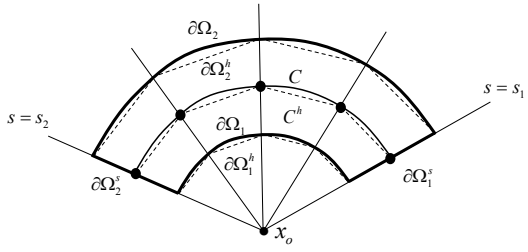


Figure 3. Schematic of a generic body $\Omega$ and its approximation $\Omega^h$

As a result of the boundary partition $\partial\Omega = \partial\Omega_1 \cup \partial\Omega_2 \cup \partial\Omega^s_1 \cup \partial\Omega^s_1$, by changing to the $\xi, s$-coordinates via the transformation, the weak-form in Eq. (5) becomes

$$\begin{aligned} \int_{s_1}^{s_2}\int_{\xi_1}^{\xi_2} (\mathbf{Lw})^T\mathbf{D}(\mathbf{Lu})J\xi d\xi ds = &\int_{s_1}^{s_2} \mathbf{w}_1^T\mathbf{t}_1(s)J^s(s)\xi_1 ds + \int_{s_1}^{s_2} \mathbf{w}_2^T\mathbf{t}_2(s)J^s(s)\xi_2 ds \\ &+ \int_{\xi_1}^{\xi_2} (\mathbf{w}_1^s)^T\mathbf{t}_1^s(\xi)J_1^\xi d\xi + \int_{\xi_1}^{\xi_2} (\mathbf{w}_2^s)^T\mathbf{t}_2^s(\xi)J_2^\xi d\xi + \int_{s_1}^{s_2}\int_{\xi_1}^{\xi_2} \mathbf{w}^T\mathbf{b}J\xi d\xi ds \end{aligned} \tag{13}$$

By manipulating the involved matrix algebra, integrating the first two integrals by parts with respect to the coordinate $\xi$, the weak-form in Eq. (13) is approximated by

$$\begin{aligned}&\int_{\xi_1}^{\xi_2} (\mathbf{W}^h)^T \left[-\xi\mathbf{E}_0\mathbf{U}^h_{,\xi\xi} + (\mathbf{E}_1 - \mathbf{E}_1^T - \mathbf{E}_0)\mathbf{U}^h_{,\xi} + \frac{1}{\xi}\mathbf{E}_2\mathbf{U}^h - \mathbf{F}_t - \xi\mathbf{F}_b\right]d\xi \\ &+ (\mathbf{W}_2^h)^T \left[\left\{\xi\mathbf{E}_0\mathbf{U}^h_{,\xi} + \mathbf{E}_1^T\mathbf{U}^h\right\}_{\xi=\xi_2} - \mathbf{P}_2\right] - (\mathbf{W}_1^h)^T \left[\left\{\xi\mathbf{E}_0\mathbf{U}^h_{,\xi} + \mathbf{E}_1^T\mathbf{U}^h\right\}_{\xi=\xi_1} + \mathbf{P}_1\right] = 0\end{aligned} \tag{14}$$

where the matrices $\mathbf{E}_0$, $\mathbf{E}_1$, $\mathbf{E}_2$, and the following quantities are defined by

$$\mathbf{E}_0 = \int_{\xi_1}^{\xi_2} \mathbf{B}_1^T\mathbf{D}\mathbf{B}_1 J ds; \quad \mathbf{E}_1 = \int_{\xi_1}^{\xi_2} \mathbf{B}_2^T\mathbf{D}\mathbf{B}_1 J d; \quad \mathbf{E}_2 = \int_{\xi_1}^{\xi_2} \mathbf{B}_2^T\mathbf{D}\mathbf{B}_2 J ds \tag{15}$$

$$\mathbf{P}_1 = \int_{s_i}^{s_o} (\mathbf{N}^S)^T\mathbf{t}_1(s)\xi_1 J^s(s) ds; \quad \mathbf{P}_2 = \int_{s_i}^{s_o} (\mathbf{N}^S)^T\mathbf{t}_2(s)\xi_2 J^s(s) ds \tag{16}$$

$$\mathbf{F}_1^t = \mathbf{F}_1^t(\xi) = (\mathbf{N}_1^S)^T\mathbf{t}_1^s(\xi)J_1^\xi; \quad \mathbf{F}_2^t = \mathbf{F}_2^t(\xi) = (\mathbf{N}_2^S)^T\mathbf{t}_2^s(\xi)J_2^\xi; \quad \mathbf{F}^t = \mathbf{F}_1^t + \mathbf{F}_2^t \tag{17}$$

$$\mathbf{F}^b = \mathbf{F}^b(\xi) = \int_{s_1}^{s_2} (\mathbf{N}^S)^T\mathbf{b} J ds \tag{18}$$

From the arbitrariness of the weight function $\mathbf{W}^h$, it can be deduced that

$$\xi^2\mathbf{E}_0\mathbf{U}^h_{,\xi\xi} + \xi(\mathbf{E}_0 + \mathbf{E}_1^T - \mathbf{E}_1)\mathbf{U}^h_{,\xi} - \mathbf{E}_2\mathbf{U}^h + \xi\mathbf{F}^t + \xi^2\mathbf{F}^b = \mathbf{0} \quad \forall\xi \in (\xi_1, \xi_2) \tag{19}$$

$$\mathbf{Q}^h(\xi_2) = \mathbf{P}_2 \tag{20}$$

$$\mathbf{Q}^h(\xi_1) = -\mathbf{P}_1 \tag{21}$$

where the vector $\mathbf{Q}^h = \mathbf{Q}^h(\xi)$ commonly known as the nodal internal flux is defined by

$$\mathbf{Q}^h(\xi) = \xi\mathbf{E}_0\mathbf{U}^h_{,\xi} + \mathbf{E}_1^T\mathbf{U}^h \tag{22}$$

Eqs. (19)–(21) form a set of the so-called scaled boundary finite element equations governing the function $\mathbf{U}^h = \mathbf{U}^h(\xi)$. It can be remarked that Eq. (19) forms a system of linear, second-order, non-homogeneous, ordinary differential equations with respect to the coordinate $\xi$ whereas Eqs. (20) and (21) pose the boundary conditions on the inner and outer boundaries of the body. It should be evident from Eqs. (19)–(21) that the information associated with the prescribed distributed body source and the prescribed boundary conditions on both inner and outer boundaries can be integrated into the formulation via the term $\mathbf{F}^b$ and the conditions described in Eqs. (20) and (21), respectively. Consistent with the partition of the vector $\mathbf{U}^h$, the vector $\mathbf{F}^t$ can also be partitioned into $\mathbf{F}^t = \{\mathbf{F}^{tu} \quad \mathbf{F}^{tc}\}^T$ where $\mathbf{F}^{tu} = \mathbf{F}^{tu}(\xi)$ contains many $\mathbf{0}$ functions and known functions associated with prescribed surface flux on the side face and has the same dimension as that of $\mathbf{U}^{hu}$ and $\mathbf{F}^{tc} = \mathbf{F}^{tc}(\xi)$ contains unknown functions associated with the unknown surface flux on the side face and has the same dimension as that of

$\mathbf{U}^{hc}$. According to this partition, the system of differential equations in Eq. (19) and the nodal internal flux can be expressed, in a partitioned form, as

$$\xi^2\begin{bmatrix} \mathbf{E}_0^{uu} & \mathbf{E}_0^{uc} \\ (\mathbf{E}_0^{uc})^T & \mathbf{E}_0^{cc} \end{bmatrix}\begin{Bmatrix} \mathbf{U}_{,\xi\xi}^{hu} \\ \mathbf{U}_{,\xi\xi}^{hc} \end{Bmatrix} + \xi\begin{bmatrix} \mathbf{E}_0^{uu} + (\mathbf{E}_1^{uu})^T - \mathbf{E}_1^{uu} & \mathbf{E}_0^{uc} + (\mathbf{E}_1^{cu})^T - \mathbf{E}_1^{uc} \\ (\mathbf{E}_0^{uc})^T + (\mathbf{E}_1^{uc})^T - \mathbf{E}_1^{cu} & \mathbf{E}_0^{cc} + (\mathbf{E}_1^{cc})^T - \mathbf{E}_1^{cc} \end{bmatrix}\begin{Bmatrix} \mathbf{U}_{,\xi}^{hu} \\ \mathbf{U}_{,\xi}^{hc} \end{Bmatrix} - \begin{bmatrix} \mathbf{E}_2^{uu} & \mathbf{E}_2^{uc} \\ (\mathbf{E}_2^{uc})^T & \mathbf{E}_2^{cc} \end{bmatrix}\begin{Bmatrix} \mathbf{U}^{hu} \\ \mathbf{U}^{hc} \end{Bmatrix} + \xi\begin{Bmatrix} \mathbf{F}^{tu} \\ \mathbf{F}^{tc} \end{Bmatrix} + \xi^2\begin{Bmatrix} \mathbf{F}^{bu} \\ \mathbf{F}^{bc} \end{Bmatrix} = \mathbf{0} \tag{23}$$

$$\begin{Bmatrix} \mathbf{Q}^{hu} \\ \mathbf{Q}^{hc} \end{Bmatrix} = \xi\begin{bmatrix} \mathbf{E}_0^{uu} & \mathbf{E}_0^{uc} \\ (\mathbf{E}_0^{uc})^T & \mathbf{E}_0^{cc} \end{bmatrix}\begin{Bmatrix} \mathbf{U}_{,\xi}^{hu} \\ \mathbf{U}_{,\xi}^{hc} \end{Bmatrix} + \begin{bmatrix} (\mathbf{E}_1^{uu})^T & (\mathbf{E}_1^{cu})^T \\ (\mathbf{E}_1^{uc})^T & (\mathbf{E}_1^{cc})^T \end{bmatrix}\begin{Bmatrix} \mathbf{U}^{hu} \\ \mathbf{U}^{hc} \end{Bmatrix} \tag{24}$$

Eq. (23) can be separated into two systems:

$$\xi^2\mathbf{E}_0^{uu}\mathbf{U}_{,\xi\xi}^{hu} + \xi\left[\mathbf{E}_0^{uu} + (\mathbf{E}_1^{uu})^T - \mathbf{E}_1^{uu}\right]\mathbf{U}_{,\xi}^{hu} - \mathbf{E}_2^{uu}\mathbf{U}^{hu} = -\xi\mathbf{F}^{tu} - \xi^2\mathbf{F}^{bu} - \mathbf{F}^{suu} \tag{25}$$

$$\xi\mathbf{F}^{tc} = -\xi^2\mathbf{F}^{bc} - \mathbf{F}^{suc} - \mathbf{F}^{scc} \tag{26}$$

where the vectors $\mathbf{F}^{suu}$, $\mathbf{F}^{suc}$, and $\mathbf{F}^{scc}$ are defined by

$$\mathbf{F}^{suu} = \xi^2\mathbf{E}_0^{uc}\mathbf{U}_{,\xi\xi}^{hc} + \xi(\mathbf{E}_0^{uc} + (\mathbf{E}_1^{cu})^T - \mathbf{E}_1^{uc})\mathbf{U}_{,\xi}^{hc} - \mathbf{E}_2^{uc}\mathbf{U}^{hc} \tag{27}$$

$$\mathbf{F}^{suc} = \xi^2(\mathbf{E}_0^{uc})^T\mathbf{U}_{,\xi\xi}^{hu} + \xi\left[(\mathbf{E}_0^{uc})^T + (\mathbf{E}_1^{uc})^T - \mathbf{E}_1^{cu}\right]\mathbf{U}_{,\xi}^{hu} - (\mathbf{E}_2^{uc})^T\mathbf{U}^{hu} \tag{28}$$

$$\mathbf{F}^{scc} = \xi^2\mathbf{E}_0^{cc}\mathbf{U}_{,\xi\xi}^{hc} + \xi\left[\mathbf{E}_0^{cc} + (\mathbf{E}_1^{cc})^T - \mathbf{E}_1^{cc}\right]\mathbf{U}_{,\xi}^{hc} - \mathbf{E}_2^{cc}\mathbf{U}^{hc} \tag{29}$$

By following the same procedure, the partitioned equation as shown in Eq. (24) can also be separated into two systems:

$$\mathbf{Q}^{hu}(\xi) = \xi\mathbf{E}_0^{uu}\mathbf{U}_{,\xi}^{hu} + (\mathbf{E}_1^{uu})^T\mathbf{U}^{hu} + \mathbf{Q}^{huc}(\xi) \tag{30}$$

$$\mathbf{Q}^{hc}(\xi) = \xi(\mathbf{E}_0^{uc})^T\mathbf{U}_{,\xi}^{hu} + (\mathbf{E}_1^{uc})^T\mathbf{U}^{hu} + \mathbf{Q}^{hcc}(\xi) \tag{31}$$

where the known vectors $\mathbf{Q}^{huc}(\xi)$ and $\mathbf{Q}^{hcc}(\xi)$ are defined by

$$\mathbf{Q}^{huc}(\xi) = \xi\mathbf{E}_0^{uc}\mathbf{U}_{,\xi}^{hc} + (\mathbf{E}_1^{cu})^T\mathbf{U}^{hc}; \quad \mathbf{Q}^{huc}(\xi) = \xi\mathbf{E}_0^{cc}\mathbf{U}_{,\xi}^{hc} + (\mathbf{E}_1^{cc})^T\mathbf{U}^{hc} \tag{32}$$

Now, a system of differential equations given by Eq. (25) along with the following two boundary conditions on the inner and outer boundaries:

$$\mathbf{Q}^{hu}(\xi_2) = \mathbf{P}_2^u \tag{33}$$

$$\mathbf{Q}^{hu}(\xi_1) = -\mathbf{P}_1^u \tag{34}$$

A homogeneous solution of the system of linear differential equations in Eq. (25), denoted by $\mathbf{U}_0^{hu}$, is derived following standard procedure from the theory of differential equations. The homogeneous solution $\mathbf{U}_0^{hu}$ must satisfy

$$\xi^2\mathbf{E}_0^{uu}\mathbf{U}_{0,\xi\xi}^{hu} + \xi\left[\mathbf{E}_0^{uu} + (\mathbf{E}_1^{uu})^T - \mathbf{E}_1^{uu}\right]\mathbf{U}_{0,\xi}^{hu} - \mathbf{E}_2^{uu}\mathbf{U}_0^{hu} = \mathbf{0} \tag{35}$$

and the corresponding nodal internal flux, denoted by $\mathbf{Q}_0^{hu}(\xi)$, is given by

$$\mathbf{Q}_0^{hu}(\xi) = \xi\mathbf{E}_0^{uu}\mathbf{U}_{0,\xi}^{hu} + (\mathbf{E}_1^{uu})^T\mathbf{U}_0^{hu} \tag{36}$$

Since Eq. (35) is a set of $(m-p)\Lambda$ linear, second-order, Euler-Cauchy differential equations, the solution $\mathbf{U}_0^{hu}$ takes the following form

$$\mathbf{U}_0^{hu}(\xi) = \sum_{i=1}^{2(m-p)\Lambda} c_i \xi^{\lambda_i} \boldsymbol{\psi}_i^u \tag{37}$$

where a constant $\lambda_i$ is termed the modal scaling factor, $\boldsymbol{\psi}$ is the $(m-p)\Lambda$-component vector representing the $i^{th}$ mode of the state variable, and $c_i$ are arbitrary constants denoting the contribution of each mode to the solution. By substituting Eq. (37) into Eqs. (35) and (36), then introducing a $2(m-p)\Lambda$-component vector $\mathbf{X}_i$ such that $\mathbf{X}_i = \{\boldsymbol{\psi}_i^u \quad \mathbf{q}_i^u\}^T$, Eqs. (35) and (36) can be combined into a system of linear algebraic equations

$$\mathbf{A}\mathbf{X}_i = \lambda_i \mathbf{X}_i \tag{38}$$

where the matrix $\mathbf{A}$ is given by

$$\mathbf{A} = \begin{bmatrix} -(\mathbf{E}_0^{uu})^{-1}(\mathbf{E}_1^{uu})^T & (\mathbf{E}_0^{uu})^{-1} \\ \mathbf{E}_2^{uu} - \mathbf{E}_1^{uu}(\mathbf{E}_0^{uu})^{-1}(\mathbf{E}_1^{uu})^T & \mathbf{E}_1^{uu}(\mathbf{E}_0^{uu})^{-1} \end{bmatrix} \tag{39}$$

Determination of all $2(m-p)\Lambda$ pairs $\{\lambda_i, \mathbf{X}_i\}$ is achieved by solving the eigenvalue problem in Eq. (38) where $\lambda_i$ denote the eigenvalues and $\mathbf{X}_i$ are associated eigenvectors. In fact, only a half of the eigenvalues has the positive real part whereas the other half has negative real part. Let $\boldsymbol{\lambda}^+$ and $\boldsymbol{\lambda}^-$ be $(m-p)\Lambda \times (m-p)\Lambda$ diagonal matrices containing eigenvalues with the positive real part and the negative real part, respectively. Also, let $\boldsymbol{\Phi}^{\psi+}$ and $\boldsymbol{\Phi}^{q+}$ be matrices whose columns containing, respectively, all vectors $\boldsymbol{\psi}_i^u$ and $\mathbf{q}_i^u$ obtained from the eigenvectors $\mathbf{X}_i = \{\boldsymbol{\psi}_i^u \quad \mathbf{q}_i^u\}^T$ associated with all eigenvalues contained in $\boldsymbol{\lambda}^+$ and let $\boldsymbol{\Phi}^{\psi-}$ and $\boldsymbol{\Phi}^{q-}$ be matrices whose columns containing, respectively, all vectors $\boldsymbol{\psi}_i^u$ and $\mathbf{q}_i^u$ obtained from the eigenvectors $\mathbf{X}_i = \{\boldsymbol{\psi}_i^u \quad \mathbf{q}_i^u\}^T$ associated with all eigenvalues contained in $\boldsymbol{\lambda}^-$. Now, the homogeneous solutions $\mathbf{U}_0^{hu}$ and $\mathbf{Q}_0^{hu}(\xi)$ are given by

$$\mathbf{U}_0^{hu}(\xi) = \boldsymbol{\Phi}^{\psi+}\boldsymbol{\Pi}^+(\xi)\mathbf{C}^+ + \boldsymbol{\Phi}^{\psi-}\boldsymbol{\Pi}^-(\xi)\mathbf{C}^- \tag{40}$$

$$\mathbf{Q}_0^{hu}(\xi) = \boldsymbol{\Phi}^{q+}\boldsymbol{\Pi}^+(\xi)\mathbf{C}^+ + \boldsymbol{\Phi}^{q-}\boldsymbol{\Pi}^-(\xi)\mathbf{C}^- \tag{41}$$

where $\boldsymbol{\Pi}^+$ and $\boldsymbol{\Pi}^-$ are diagonal matrices obtained by simply replacing the diagonal entries $\lambda_i$ of the matrices $\lambda^+$ and $\lambda^-$ by the a function $\xi^{\lambda_i}$, respectively; and $\mathbf{C}^+$ and $\mathbf{C}^-$ are vectors containing arbitrary constants representing the contribution of each mode. It is apparent that the diagonal entries of $\boldsymbol{\Pi}^+$become infinite when $\xi \to \infty$ whereas those of $\boldsymbol{\Pi}^-$is unbounded when $\xi \to 0$. As a result, $\mathbf{C}^+$ is taken to $\mathbf{0}$ to ensure the boundedness of the solution for unbounded bodies and, similarly, the condition $\mathbf{C}^- = 0$ is enforced for bodies containing the scaling center.

A particular solution of Eq. (25), denoted by $\mathbf{U}_1^{hu}$, associated with the distributed body source, the surface flux on the side face and the prescribed state variable on the side face can also be obtained from a standard procedure in the theory of differential equations such as the method of undetermined coefficient. Once the particular solution $\mathbf{U}_1^{hu}$ is obtained, the corresponding particular nodal internal flux $\mathbf{Q}_1^{hu}$ can be calculated. Finally, the general solution of Eq. (25) and the corresponding nodal internal flux are then given by

$$\mathbf{U}^{hu}(\xi) = \mathbf{U}_0^{hu}(\xi) + \mathbf{U}_1^{hu}(\xi) = \boldsymbol{\Phi}^{\psi+}\boldsymbol{\Pi}^+(\xi)\mathbf{C}^+ + \boldsymbol{\Phi}^{\psi-}\boldsymbol{\Pi}^-(\xi)\mathbf{C}^- + \mathbf{U}_1^{hu}(\xi) \tag{42}$$

$$\mathbf{Q}^{hu}(\xi) = \mathbf{Q}_0^{hu}(\xi) + \mathbf{Q}_1^{hu}(\xi) = \boldsymbol{\Phi}^{q+}\boldsymbol{\Pi}^+(\xi)\mathbf{C}^+ + \boldsymbol{\Phi}^{q-}\boldsymbol{\Pi}^-(\xi)\mathbf{C}^- + \mathbf{Q}_1^{hu}(\xi) \tag{43}$$

To determine the constants contained in $\mathbf{C}^+$ and $\mathbf{C}^-$, the boundary conditions on both inner and outer boundaries are enforced. By enforcing the conditions Eqs. (33) and (34), it gives rise to

$$\left\{ \begin{array}{c} \mathbf{C}^+ \\ \mathbf{C}^- \end{array} \right\} = \left[ \begin{array}{cc} \mathbf{\Phi}^{q+}\mathbf{\Pi}^+(\xi_1) & \mathbf{\Phi}^{q-}\mathbf{\Pi}^-(\xi_1) \\ \mathbf{\Phi}^{q+}\mathbf{\Pi}^+(\xi_2) & \mathbf{\Phi}^{q-}\mathbf{\Pi}^-(\xi_2) \end{array} \right]^{-1} \left( \left\{ \begin{array}{c} -\mathbf{P}_1^u \\ \mathbf{P}_2^u \end{array} \right\} - \left\{ \begin{array}{c} \mathbf{Q}_1^{hu}(\xi_1) \\ \mathbf{Q}_1^{hu}(\xi_2) \end{array} \right\} \right) \tag{44}$$

From Eq. (44), it can readily be obtained and substituting Eq. (47) into its yields

$$\mathbf{K} \left\{ \begin{array}{c} \mathbf{U}^{hu}(\xi_1) \\ \mathbf{U}^{hu}(\xi_2) \end{array} \right\} = \left\{ \begin{array}{c} -\mathbf{P}_1^u \\ \mathbf{P}_2^u \end{array} \right\} + \mathbf{K} \left\{ \begin{array}{c} \mathbf{U}_1^{hu}(\xi_1) \\ \mathbf{U}_1^{hu}(\xi_2) \end{array} \right\} - \left\{ \begin{array}{c} \mathbf{Q}_1^{hu}(\xi_1) \\ \mathbf{Q}_1^{hu}(\xi_2) \end{array} \right\} \tag{45}$$

where the coefficient matrix $\mathbf{K}$, commonly termed the stiffness matrix, is given by

$$\mathbf{K} = \left[ \begin{array}{cc} \mathbf{\Phi}^{q+}\mathbf{\Pi}^+(\xi_1) & \mathbf{\Phi}^{q-}\mathbf{\Pi}^-(\xi_1) \\ \mathbf{\Phi}^{q+}\mathbf{\Pi}^+(\xi_2) & \mathbf{\Phi}^{q-}\mathbf{\Pi}^-(\xi_2) \end{array} \right] \left[ \begin{array}{cc} \mathbf{\Phi}^{\psi+}\mathbf{\Pi}^+(\xi_1) & \mathbf{\Phi}^{\psi-}\mathbf{\Pi}^-(\xi_1) \\ \mathbf{\Phi}^{\psi+}\mathbf{\Pi}^+(\xi_2) & \mathbf{\Phi}^{\psi-}\mathbf{\Pi}^-(\xi_2) \end{array} \right]^{-1} \tag{46}$$

(for more details about the method procedure, see also the work of [13]).

By applying the prescribed surface flux and the state variable on both inner and outer boundaries, a system of linear algebraic equations as shown in Eq. (25) is sufficient for determining all involved unknowns. Once the unknowns on both the inner and outer boundaries are solved, the approximate field quantities such as the state variable and the surface flux within the body can readily be post-processed, and the approximated body flux can be computed from (10) and (11) as

$$\mathbf{u}^h(\xi, s) = \mathbf{N}^S(s)\mathbf{U}^h(\xi) = \mathbf{N}^{Su}(s)\mathbf{U}^{hu}(\xi) + \mathbf{N}^{Sc}(s)\mathbf{U}^{hc}(\xi) \tag{47}$$

$$\boldsymbol{\sigma}^h(\xi, s) = \mathbf{D}\left[\mathbf{B}_1^u(s)\mathbf{U}_{,\xi}^{hu}(\xi) + \frac{1}{\xi}\mathbf{B}_2^u(s)\mathbf{U}^{hu}(\xi)\right] + \mathbf{D}\left[\mathbf{B}_1^c(s)\mathbf{U}_{,\xi}^{hc}(\xi) + \frac{1}{\xi}\mathbf{B}_2^c(s)\mathbf{U}^{hc}(\xi)\right] \tag{48}$$

where $\mathbf{N}^{Su}$ and $\mathbf{N}^{Sc}$ are matrices resulting from the partition of $\mathbf{N}^S$; $\mathbf{B}_1^u$, $\mathbf{B}_1^c$ and $\mathbf{B}_2^u$, $\mathbf{B}_2^c$ are matrices resulting from the partition of the matrices $\mathbf{B}_1$ and $\mathbf{B}_2$, respectively. It is emphasized here again that the solutions in Eqs. (47) and (48) also apply to the special cases of bounded and unbounded bodies. For bounded bodies containing the scaling center, $\mathbf{C}^-$ simply vanishes and, for unbounded bodies, $\mathbf{C}^+ = \mathbf{0}$.

## 4. Performance application

Based on the method procedure of the prosed technique, numerical technique is written in Matlab by the author. Some numerical examples to verify the proposed technique and demonstrate its performance and capabilities. To demonstrate its capability to treat a variety of boundary value problems, general boundary conditions, and prescribed data on the side faces, the types of problems associated with linear elasticity ($\Lambda = 2$) for various scenarios within the context of geo-mechanics applications. The conventional polar coordinates are utilized to achieve the exact description of the circular defining curve, exact geometry of domain. The number of meshes with $N$ identical linear elements are employed. The number of meshes are the number of elements on defining curve. The accuracy and convergence of numerical solutions are carrying out the analysis via a series of meshes.

### *4.1. Semi-circular hole in an infinite domain*

Consider a semi-circular hole of radius $R$ in an infinite domain as shown in Fig. 4(a). The medium is made of a homogeneous, linearly elastic, isotropic material with Young's modulus $E$ and Poisson's ratio $\nu$ and subjected to the pressure $p_1 = p\cos\phi$ on the surface of the hole, and the modulus matrix $\mathbf{D}$ with non-zero entries $D_{11} = (1-\nu)E/(1+\nu)(1-2\nu)$, $D_{44} = (1-\nu)E/(1+\nu)(1-2\nu)$, $D_{14} = D_{41} = \nu E/(1+\nu)(1-2\nu)$, $D_{23} = E/2(1+\nu)$, $D_{22} = E/2(1+\nu)$, $D_{32} = E/2(1+\nu)$, $D_{33} = E/2(1+\nu)$. Due to the symmetry, it is sufficient to model this problem using only half of the semi-circular as shown in Fig. 4(b), with appropriate condition on side face (i.e., the normal displacement and tangential traction on the side faces vanish). To describe the geometry, the scaling center is chosen at the center of the semi-circular whereas the hole boundary is treated as the defining curve. In a numerical study, the Poisson's ratio $\nu = 0.3$ and meshes with $N$ identical linear elements are employed.

Results for normalized radial stress ($\sigma_{rr}/p_1$) is reported in Fig. 5, respectively, for four meshes (i.e., $N = 4, 8, 16, 32$). It is worth noting that the discretization with only few linear elements can capture numerical solution with the sufficient accuracy.

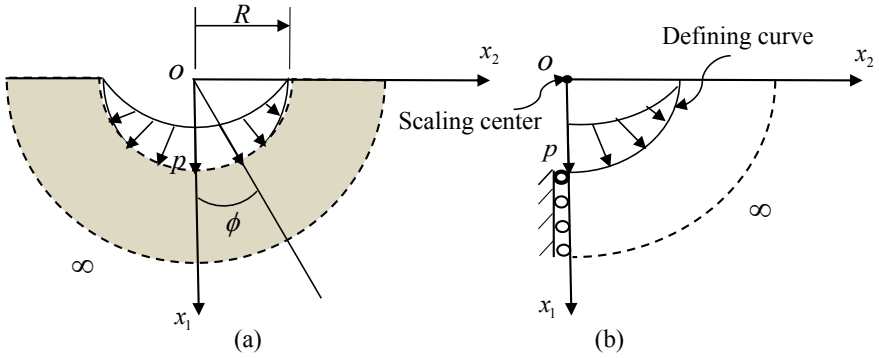


Figure 4. Schematics of (a) pressurized semi-circular hole in linear elastic, infinite medium and (b) half of domain used in the analysis

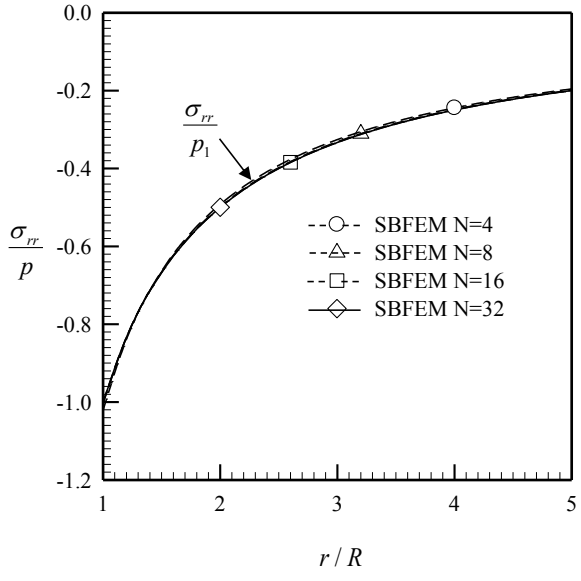


Figure 5. Normalized radial stress component along the radial direction of semi-circular hole in linear elastic, infinite medium at coordinate

### 4.2. *Semi-infinite wedge*

As the last example, a representative boundary value problem associated with a semi-infinite wedge is considered in order to investigate the capability of the proposed technique as shown in Fig. 6(a). The medium is made of a homogeneous, linearly elastic, isotropic material with Young's modulus $E$ and Poisson's ratio $\nu$ and subjected to the uniform pressure $p$ on the surface of the $x_2$ direction, (the modulus matrix $\mathbf{D}$ is taken to be same as that employed in section 4.1 for the plane strain condition). In the geometry modeling, the scaling center is considered at 0. The geometry of semi-infinite is fully described by the defining curve on hole of domain. As a result, the two boundaries become the side faces (Fig. 6(b)). In the analysis, the Poisson's ratio is taken as $\nu = 0.3$ and defining curve is discretized by $N$ identical linear elements. The normalized radial stress ($\sigma_{rr}/\nu p$) and normalized hoop stress ($\sigma_{\theta\theta}/\nu p$) are reported along radial (angle $\theta/2$) in Figs. 7 and 8. It can be seen that the discretization with only few linear elements can capture numerical solution with the sufficient accuracy.

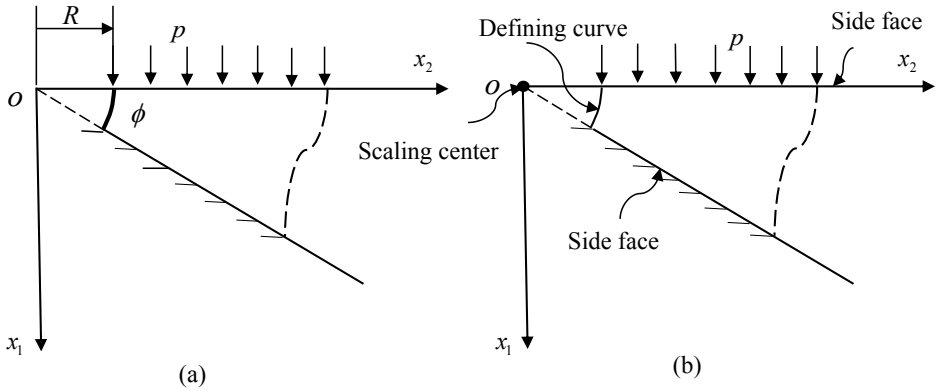


Figure 6. Schematics of (a) semi-infinite wedge in linear elastic, infinite medium and (b) domain used in the analysis

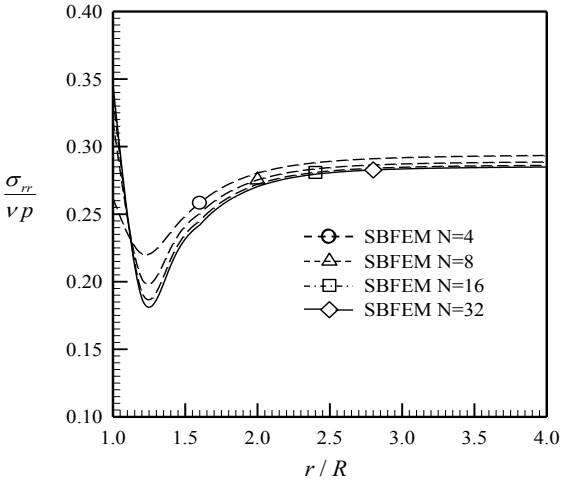


Figure 7. Normalized radial stress component along the radial direction of pressurized circular hole in linear elastic, infinite medium

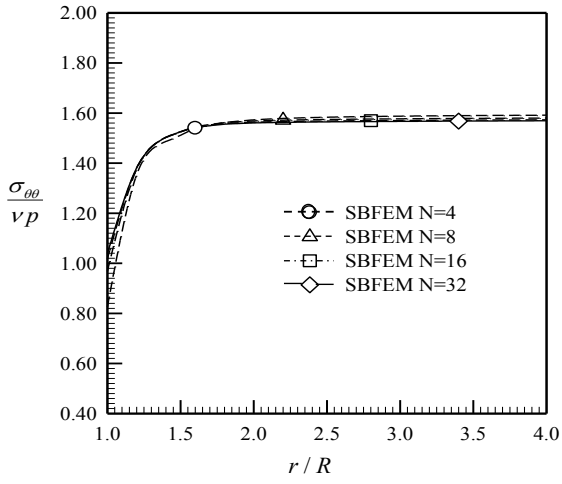


Figure 8. Normalized hoop stress component along the radial direction of pressurized circular hole in linear elastic, infinite medium

## 5. Conclusions

A numerical technique based on the scaled boundary finite element method has been successfully developed for solving two-dimensional, multi-field boundary value problems with the domain completely described by a circular defining curve. Both the formulation and implementations have been established in a general framework allowing a variety of linear boundary value problems and the general associated data (such as the domain geometry, the prescribed distributed body source, boundary conditions, and contribution of the side face) to be treated in a single, unified fashion. Results from several numerical study have indicated that the proposed SBFEM yields highly accurate numerical solutions with the percent error weakly dependent on the level of mesh refinement. The results also show that it is advantageous to use circular defining curve, and that higher convergence can be obtained. The potential extension of the proposed technique will be developed to investigate the mechanical behavior of geomaterials such as anisotropic, non-linear and elastoplastic.

## References


[1] Wolf, J. P. (2003). *The scaled boundary finite element method*. John Wiley and Sons, Chichester.

[2] Wolf, J. P., Song, C. (1996). Finite-element modelling of undounded media. In *Eleventh World Conference on Earthquake Engineering, Paper No. 70.*

[3] Song, C., Wolf, J. P. (1999). Body loads in scaled boundary finite-element method. *Computer Methods in Applied Mechanics and Engineering*, 180(1-2):117–135.

[4] Song, C., Wolf, J. P. (1997). The scaled boundary finite-element method—alias consistent infinitesimal finite-element cell method—for elastodynamics. *Computer Methods in Applied Mechanics and Engineering*, 147(3-4):329–355.

[5] Wolf, J. P., Song, C. (2001). The scaled boundary finite-element method–a fundamental solution-less boundary-element method. *Computer Methods in Applied Mechanics and Engineering*, 190(42):5551–5568.

[6] Deeks, A. J., Wolf, J. P. (2002). A virtual work derivation of the scaled boundary finite-element method for elastostatics. *Computational Mechanics*, 28(6):489–504.

[7] Deeks, A. J. (2004). Prescribed side-face displacements in the scaled boundary finite-element method. *Computers & Structures*, 82(15-16):1153–1165.

[8] Vu, T. H., Deeks, A. J. (2006). Use of higher-order shape functions in the scaled boundary finite element method. *International Journal for Numerical Methods in Engineering*, 65(10):1714–1733.

[9] Doherty, J. P., Deeks, A. J. (2005). Adaptive coupling of the finite-element and scaled boundary finite-element methods for non-linear analysis of unbounded media. *Computers and Geotechnics*, 32(6):436–444.

[10] He, Y., Yang, H., Deeks, A. J. (2012). An Element-free Galerkin (EFG) scaled boundary method. *Finite Elements in Analysis and Design*, 62:28–36.

[11] Vu, T. H., Deeks, A. J. (2008). A p-adaptive scaled boundary finite element method based on maximization of the error decrease rate. *Computational Mechanics*, 41(3):441–455.

[12] He, Y., Yang, H., Deeks, A. J. (2014). Use of Fourier shape functions in the scaled boundary method. *Engineering Analysis with Boundary Elements*, 41:152–159.

[13] Rungamornrat, J., Van, C. N. (2019). Scaled boundary finite element method with exact defining curves for two-dimensional linear multi-field media. *Frontiers of Structural and Civil Engineering*, 13(1):201–214.